REVIEW ARTICLE

HYDROGEN BALMER SERIES SPECTROSCOPY IN LASER-INDUCED BREAKDOWN PLASMAS

CHRISTIAN G. PARIGGER*

The University of Tennessee Space Institute, Center for Laser Applications, 411 B.H. Goethert Parkway, Tullahoma, TN 37388, USA

EUGENE OKS

Department of Physics, Auburn University, 206 Allison Lab, Auburn, AL 36849, USA

Abstract: A review is presented of recent experiments and diagnostics based on Stark broadening of hydrogen Balmer lines in laser-induced optical breakdown plasmas. Experiments primarily utilize pulsed Nd:YAG laser radiation at 1064-nm and nominal 10 nanosecond pulse duration. Analysis of Stark broadening and shifts in the measured H-alpha spectra, combined with Boltzmann plots from H-alpha, H-beta and H-gamma lines to infer the temperature, is discussed for the electron densities in the range of $10^{16} - 10^{19}$ cm^{-3} and for the temperatures in the range of 6,000 to 100,000 K.

Keywords: Laser-Induced Optical Breakdown, Plasma Spectroscopy, Stark Broadening.

1. INTRODUCTION

Laser-induced optical breakdown (LIOB) in atmospheric-pressure gases with nominal 10 nanosecond, 100 milliJoule/pulse laser radiation usually causes generation of electron number densities in the order of 10^{19} cm^{-3} and excitation temperatures of 100,000 K ($\approx$ 10 eV). The time-varying electron density (N_e) and electron excitation temperature (T_e) during the plasma decay can be inferred using Stark-broadening of the H-atom spectra and so-called Boltzmann plots, respectively.

The literature on Stark broadening of spectral lines in plasmas is too voluminous to be cited here. We point out only books devoted partially [1-4] or completely [5, 6] to this subject. One can use reviews of the literature in these books, especially in the three latest ones [3, 4, 6].

From the practical point of view, the most useful are Stark Broadening Tables (SBT). The earliest SBT from Griem's books [1, 5] were based on the quasistatic approximation for the ion microfield, the impact approximation for the electron microfield, and on the

assumption of no coupling of any kind between the ion and electron microfields (hereafter called Griem's SBT/theory). The SBT for hydrogen lines, where the ion dynamics and some (but not all) of the couplings between the two microfields have been taken into account, were obtained by simulations and published by Gigosos and Cardeñoso [7] and by Gigosos, González, and Cardeñoso [8] referred hereafter as the SBT/simulations by GC/GGC. More advanced SBT, based on the accurate analytical treatment of the ion dynamics and of all couplings between the ion and electron microfields, were published in 2006 by Oks [6, 9]. Oks' SBT/theory provided the best agreement with all available benchmark experiments.

Therefore, our analysis of the experimental Balmer lines observed from LIOB plasmas was based primarily on Oks' SBT/theory. For illustrating the significance of the theoretical progress, we provided also the corresponding results deduced by using Griem's SBT/theory. In some publications we employed also the SBT/simulations by GC/GGC for comparison with the corresponding results based on Oks' SBT/theory.

Application of plasma diagnostics for laser-induced optical breakdown (LIOB) for gaseous H_2 was explored

* E-mail: cparigge@tennessee.edu

in the mid-sixties [10]. A pulsed ruby laser at 694.3 nm, 30 nanosecond pulse width and 200 milliJoule/pulse was utilized for LIOB in a pressure range of 1 to 70 atm. For atmospheric pressure H_2, electron densities of 4×10^{18} cm^{-3} were inferred from Stark broadening, and excitation temperatures of 20,000 K from line-to-continuum measurements [10, 11]. Determination of N_e using relatively large Stark-broadening of the H-atom was further applied by various groups [12–17].

Plasma spectroscopy techniques [18] following LIOB have found an amazing renaissance recently. Laser-Induced Plasma Spectroscopy (LIPS) and/or Laser-induced Breakdown spectroscopy (LIBS) is now a valuable technique for determining elemental composition with the ability to analyze solids, liquids and gases with little or no sample preparation, suitable for on-site analyses [19]. The success of LIBS is in part due to the ease of availability of nominal 10-nanosecond Nd:YAG laser radiation from compact devices. Several other laser sources however have been historically applied for generation of micro-plasma with subsequent measurement methods based on use of atomic emission spectroscopy [20]. Recent interest includes applying dual- and multi- pulse excitation for the purpose of increasing sensitivity of LIBS [21]. Examples of advantages of multi-pulse excitation include an increase of the plasma volume or plasma reheating by the second pulse, in turn, enhancement of detection limits for LIBS 10- to 100-fold and/or a decrease in relative standard deviation when comparing single- with double- pulse bursts [22]. Following short-pulse uv-excitation a CO_2 laser may be used to enhance detection from a distance of atomic and molecular species [23]. Some applications are also designed with eye-safety in mind, required for remote and/or field-safe LIBS systems [24]. Applications of CO_2 lasers also include aerosol measurements [25]. In several of LIOB and/or LIBS studies hydrogen emission spectra can be discerned, allowing one to extract number density and excitation temperature. Subsequent occurrence of molecular recombination spectra allows one to further characterize laser-induced micro-plasma [26]. Moreover, increased interests in applications of LIBS are noted in Europe and North America as can be seen in the frequencies of annual meetings, e.g., Euro-Mediterranean Symposium on Laser Induced Breakdown Spectroscopy (*EMLIBS*) or North American Symposium on Laser Induced Breakdown Spectroscopy (*NASLIBS*) over and above annual or semi-annual meetings on the subject, such as Laser-Induced Breakdown Spectroscopy (*LIBS*)

conference or Laser Applications to Chemical, Security and Environmental Analysis (*LACSEA*). Fundamental results in both experiments and theory are of continued interest in application driven technologies.

In this work, we discuss time-resolved laser spectroscopy techniques to characterize the temporal evolution of the electron number density and the electron temperature of a micro-plasma generated by laser-induced optical breakdown in pure hydrogen gas [27]. Electron temperature can be inferred from Balmer series Boltzmann plots, provided that the Balmer series lines are well discernable [28]. The electron density can be determined from hydrogen Balmer-alpha and Balmer-beta lines using SBT described above. Experimental studies are reviewed of laser-generated micro plasma, including shadowgraph and time-resolved spectroscopy measurements [27–29]. Comparisons are elaborated of Oks's SBT/theory and earlier SBT/theories. Discussed are also LIOB of aluminum [30, 31] and applications of H-alpha, H-beta, and H-gamma (H_α: 6562.8 Å, H_β: 4861.4 Å, H_γ: 4340.5 Å) diagnostic of LIOB in methane [32–34]. Recent work on hydrogen-beta further elaborates details of the Stark-broadened emissions, including asymmetries in the double-peak H_β spectra [35].

2. EXPERIMENTAL DETAILS

For generation of a micro-plasma, a laboratory Nd: YAG laser operated at the fundamental wavelength of 1064 nm was used. For the hydrogen plasma investigations, a Continuum YG680S-10 Nd:YAG with 150-mJ energy per pulse and 7.5-ns pulse duration, was focused to typically 1,400 GW/cm^2 in a pressure cell that was filled with gaseous hydrogen to a pressure of 810 ± 25 Torr (1.07 × 10^5 Pa) and 1010 ± 25 Torr (1.07 × 10^5 Pa), subsequent to evacuation of the cell with a diffusion pump. In addition, a Coherent Infinity 40-100 Nd:YAG laser with 50-mJ and 300-mJ pulse energy and 3.5-ns pulse width was focused in laboratory air to an irradiance of typically 10,000 GW/cm^2. Shadowgraph images [36] of the laser-induced optical breakdown phenomena were recorded using 308-nm pulses from a 6-ns pulsed excimer laser. Optical breakdown thresholds are approximately equal for laboratory air and for gaseous hydrogen slightly above atmospheric pressure [36]. For 7.5-ns pulse width, 1064-nm Nd:YAG laser radiation, the measured air breakdown threshold is 280 ± 15 GW/cm^2.

Typical experimental arrangements include scanning spectrometer with photomultiplier or standard grating spectrometer with a diode array or 2-dimensional Charge-Coupled-Device (CCD) with an intensifier to temporally resolve hydrogen Balmer series ?emission profiles. The scanning spectrometer (Jobin-Yvon 0.64-m Czerny-Turner) and photomultiplier (RCA C41034A) arrangement, together with the Boxcar (EG and G Model 4402) allows one to record the broad hydrogen Balmer-alpha early in the plasma decay, with a spectral resolution of 0.02-nm, and with a 2-ns temporal resolution. The alternative arrangement includes an intensified diode array detector (Princeton Applied Research Corporation EG and G Model 1530-CUV) to record H_α, H_β or H_γ emission lines with a 6-ns gate for the intensifier. Synchronization is usually achieved with several delay generators (Stanford Research Systems Model DG535).

Shadowgraphs of optical breakdown in air were recorded using a 308-nm back-light radiation source (XeCl eximer laser, 6-ns pulse width) and a standard video camera. Individual breakdown events were recorded on tape. Subsequently, the images were digitized by the use of image-capture software. Figure 1 shows selected images of delays up to 10 µs of the back-light source with respect to Nd:YAG laser. The figure shows the development in time of the breakdown kernel and the onset and development in time of the shockwave. The backlight source was operated at 80 Hz; therefore, a super-position of images at two time delays is shown: at the indicated delay, and due to the double exposure at the indicated delay plus 12.5 milli-seconds. The image size is 3.6×4.8 cm. The shadowgraph technique allows one to observe the second spatial derivative, conversely, the Schlieren method reveals the refractive index gradient.
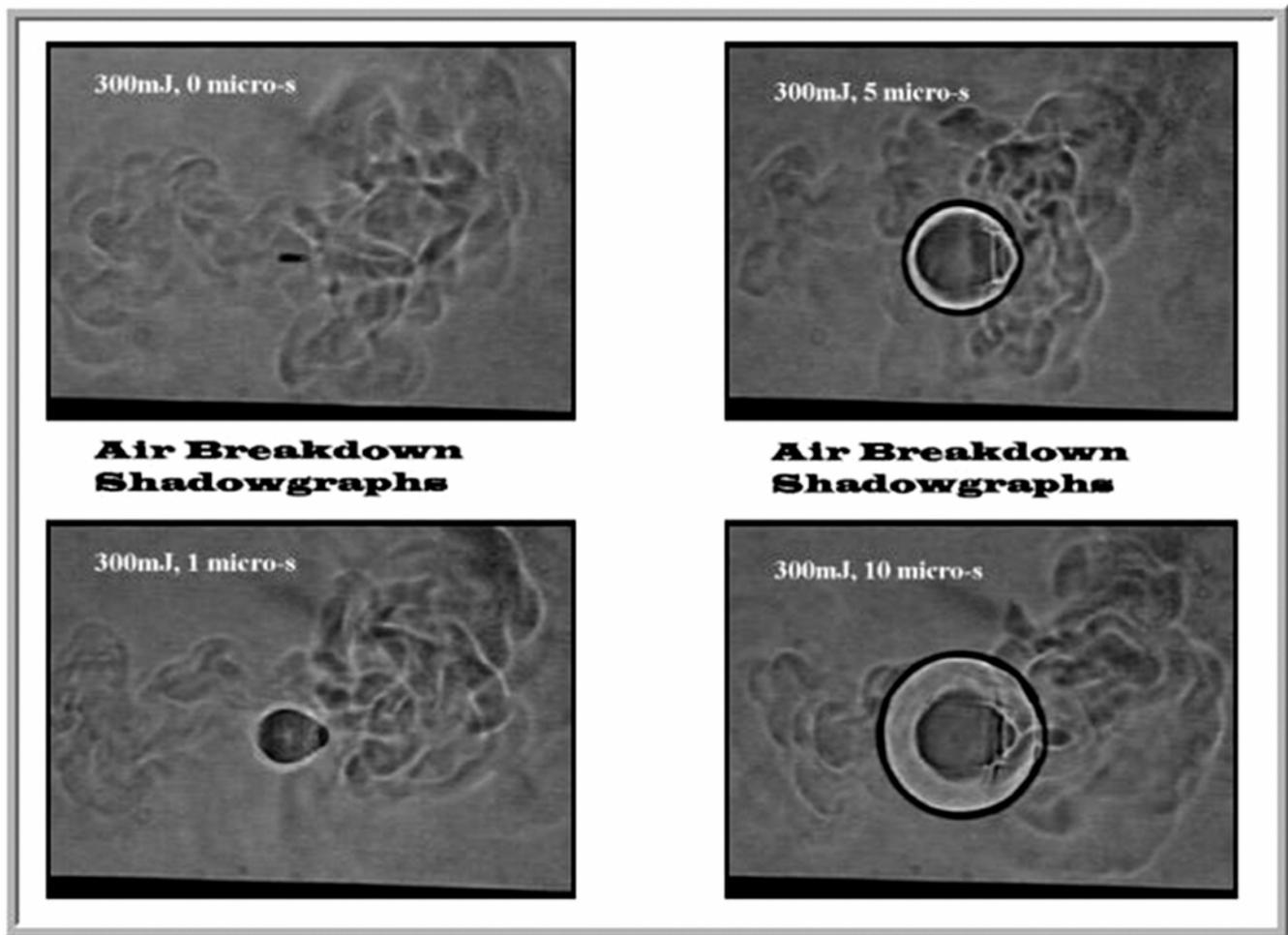
Fig. 1: Shadow graphs for time delays of $\Delta t = 0$ µs (top left), $\Delta t = 1$ µs (bottom left), $\Delta t = 5$ µs (top right), $\Delta t = 10$ µs (bottom right) for laser pulse energy of 300 mJ

The focused laser irradiance can be estimated by use of results for Gaussian beam propagation [38]. The focal spot diameter is $d_0 \approx 2 f^{\#} \lambda$, where λ is the wavelength, and the *f*-number is defined by $f^{\#} \equiv f/D$, with *f* the focal length of the lens, and *D* the diameter of the laser beam. For multimode laser radiation, the spot-size is larger by a factor *M* (the so-called *M* factor) of typically 1.4 for the YG680S-10 Nd:YAG 1064-nm laser radiation. The depth of focus or confocal parameter is given by $2z_R = 6.28 \left(f^{\#}\right)^2 \lambda$. The focal volume is $V_{focus} = 19.2 \left(f^{\#}\right)^4 \lambda^3$. The peak irradiance is $I_0 = P_0 / 2\left(f^{\#}\lambda\right)^2$, where $P_0 = 0.94 \, (Energy / pulse) / \tau_{FWHM}$ is the total power of the beam, with τ_{FWHM} the full-width at half-maximum. For example, focusing 3.5-ns pulse width, 300-mJ energy per pulse, 1064-nm radiation with $f^{\#} = 20$ (10-cm focal-length lens, 0.5 cm laser beam diameter) leads to an irradiance of $\approx 10,000 \, \text{GW/cm}^2$, a peak power of 86 MW, a depth of focus of $2z_R = 0.25$ -cm (see extent of shadow for $\approx 0 \, \mu s$ time delay, Fig. 1 top left) in a focal volume of $3 \times 10^{-6} \, \text{cm}^3$. The peak electric field strength, *E*, of a focused laser beam is calculated from $E = 27.4\sqrt{I_0}$, for *E* in volts per cm and *I* in watts per square-cm [39]. A maximum irradiance of $10,000 \, \text{GW/cm}^2$ by way of comparison is about 1/10 of the electric field strength (of $\approx 2.8 \, \text{GV/cm}$) that holds the hydrogen atom together. For the indicated irradiances of 1,400 to $10,000 \, \text{GW/cm}^2$ and the electric field strengths, plenty of optical radiation from the laser-induced plasma is available for laser induced breakdown spectroscopy. However, associated with optical breakdown is the formation of a blast wave that shows local speeds greater than 1km/s [40]. Spectroscopic data of the hydrogen Balmer lines were collected up to 3 µs after optical breakdown (see air-breakdown shadowgraphs on right side of Fig. 1). Typically molecular recombination emission spectra [41] can be measured for time delays of the order of 1 to a few 10's of microseconds after LIOB.

Figure 2, shows the measured Balmer Series hydrogen-alpha line, recorded 5-ns after generation of the optical breakdown plasma. The experimental spectrum was recorded by scanning the spectrometer and recording the signal with the photomultiplier. A 2-ns gate-width was used for the Boxcar. The measured Stark width amounts to 254 ± 35 Å, and the Stark shift is 27 ± 6 Å.

Figure 3, shows the measured Balmer series hydrogen-beta emission, 100-ns after optical breakdown. The measured Stark width amounts to 178 25 Å This spectrum was measured using the linear diode array, with a 6-ns gate-width of the intensifier.
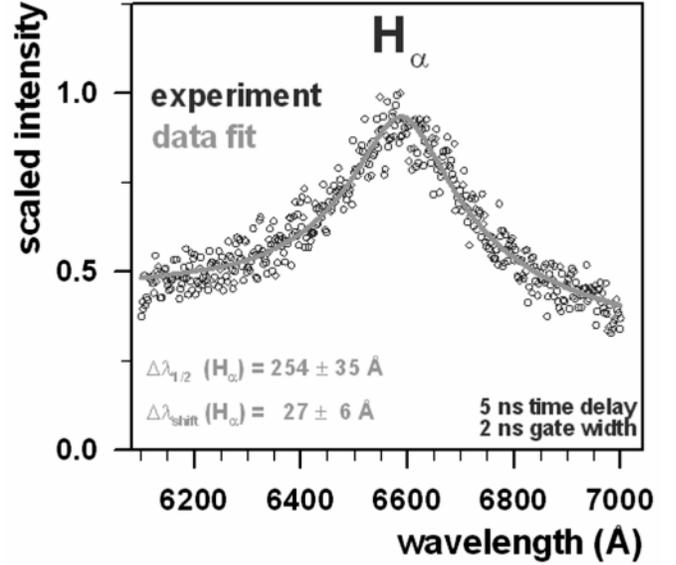

Fig. 2: Experimental hydrogen balmer-alpha line, $N_e = 85 \times 10^{17} \, \text{cm}^{-3}$
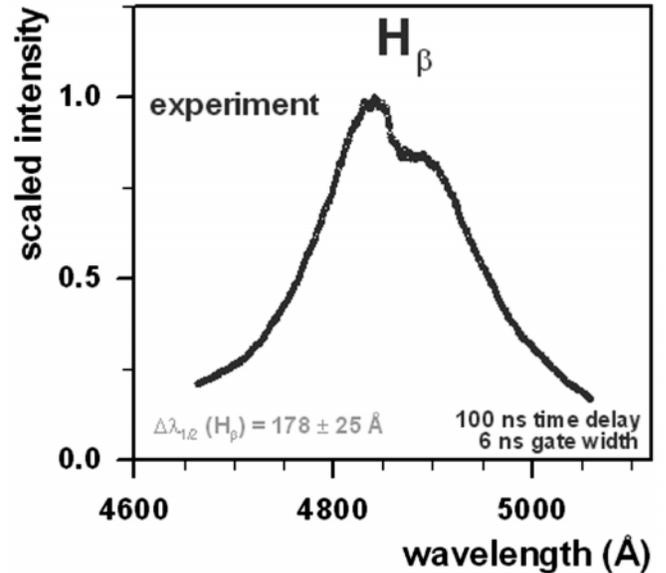

**Fig. 3:** Experimental hydrogen balmer-beta line, $N_e = 6.2 \times 10^{17} \, \text{cm}^{-3}$

In investigations of aluminum optical breakdown plasma [31], the hydrogen Balmer Series H_α and H_β lines were used as a measure for electron densities N_e. The experimental details of this work are: 45 mJ Nd: YAG ir,

12-ns pulse width radiation resulting in a peak irradiance of 300 GW/cm^2 on the aluminum target in a cell. The irradiance level is approximately a factor 3 above LIOB breakdown in air for this particular Q-switched Nd:YAG laser beam. The cell was carefully evacuated and filled to a level of 100 Torr (0.13×10^5 Pa) hydrogen gas. The time resolved spectra were recorded using a 0.5 m Acton spectrometer with a 1200 groove/mm grating. For the selected slit width the spectral resolution amounted to 0.27 nm. For the time-resolved work a 6-ns gate (or intensifier) was used in conjunction with a linear diode array and an optical multichannel analyzer.

Wavelength and sensitivity corrected data were smoothed using a 21 point, second-order Savitzky-Golay filter. Figures 4 and 5 show the results for hydrogen-alpha and beta emissions early in the plasma decay. Significant free-electron contributions are noted for the indicated time delays $\Delta\tau$, specifically for $\Delta\tau = 25$ ns for H$_\alpha$ and $\Delta\tau = 75$ ns for H$_\beta$. These recorded Balmer series lines can be used in diagnostics applications for materials processing, viz. calibrations were provided for the Stark-broadened and shifted, neutral aluminum lines Al I 394.4 nm and Al I 396.15 nm. Stark-broadening for these Al lines amounts to 0.52 ± 0.08 nm and 0.61 ± 0.08 nm, respectively; the measured shifts amount to
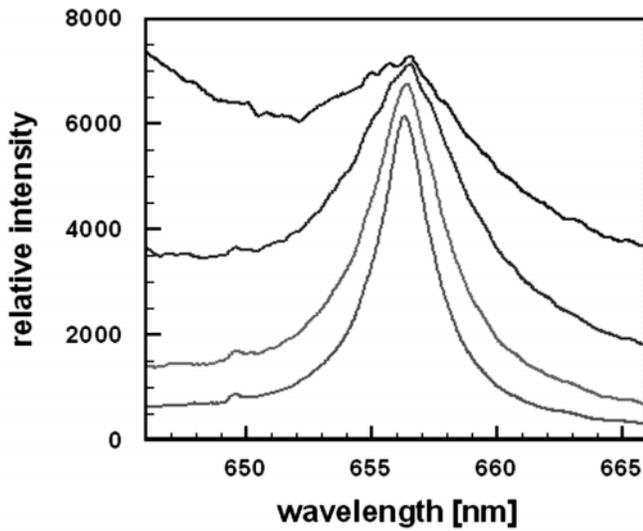
Fig. 4: Hydrogen-alpha emissions following aluminum LIOB. The measured spectra were recorded at time delays of 25, 30, 50, and 75 ns. Both width and shift of the H$_\alpha$ line were used [27] to infer N$_e$ of 10×10^{17} cm^{-3} to 3×10^{17} cm^{-3} for the indicated spectra (top to bottom)
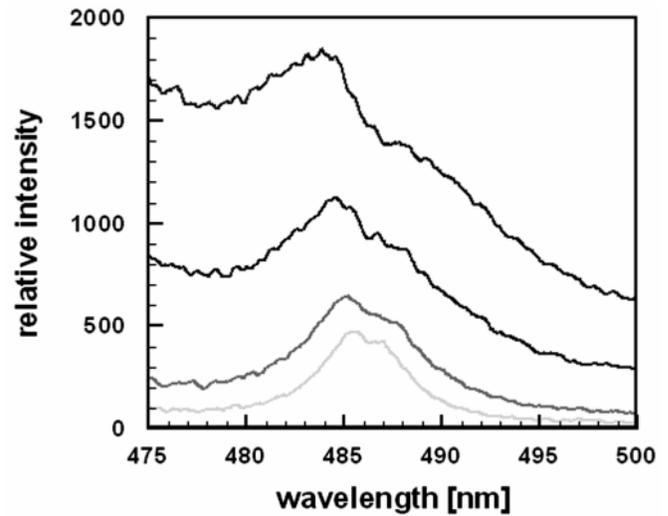
Fig. 5: Hydrogen-beta emissions following aluminum LIOB. The measured spectra were recorded at time delays of 75, 100, 150, and 200 ns. The H$_\beta$ line was used [27] to infer N$_e$ of 4×10^{17} cm^{-3} to 1×10^{17} cm^{-3} for the indicated spectra (top to bottom)


(a)

(b)
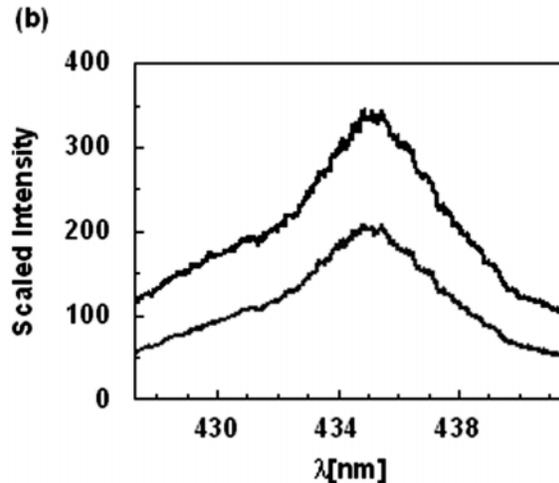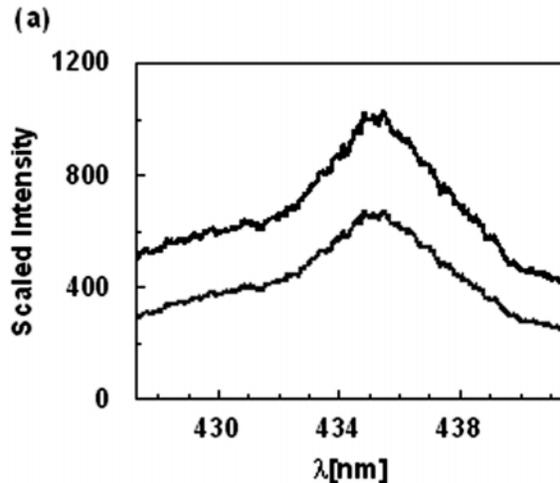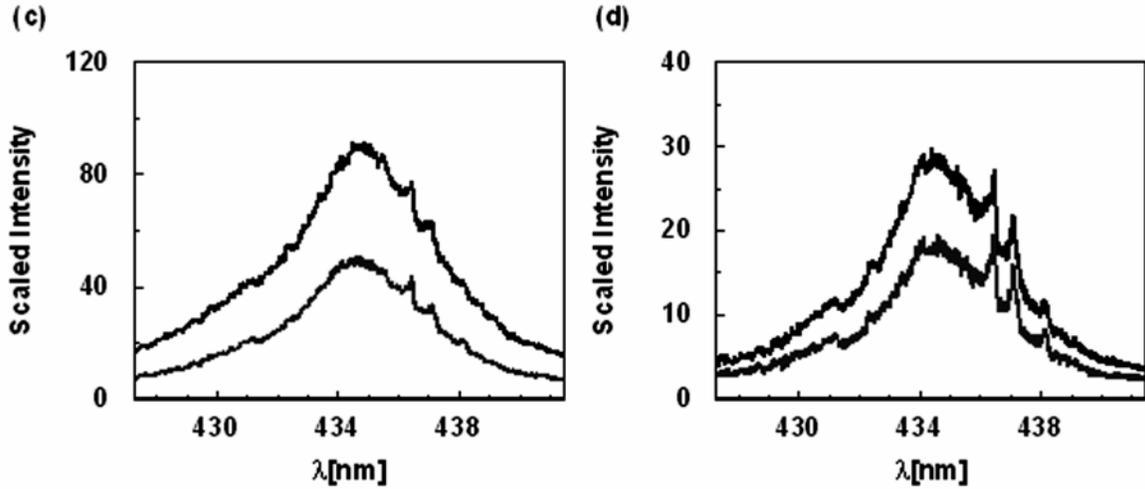
Fig. 6: Hydrogen-gamma emissions in expanding methane flow at 2.7×10^5 Pa. Time delays (a) $t_{delay} = 0.3$ µs (top), 0.4 µs, (b) $t_{delay} = 0.6$ µs (top), 0.8 µs, (c) $t_{delay} = 1.2$ µs (top), 1.5 µs, (d) $t_{delay} = 1.8$ µs (top), 2.1 µs. Note presence of the $C_2 \, d^3\Pi_g \rightarrow \Pi_u$ swan system $\Delta v = 2$ sequence for time delays > 1 µs in Figs (c) and
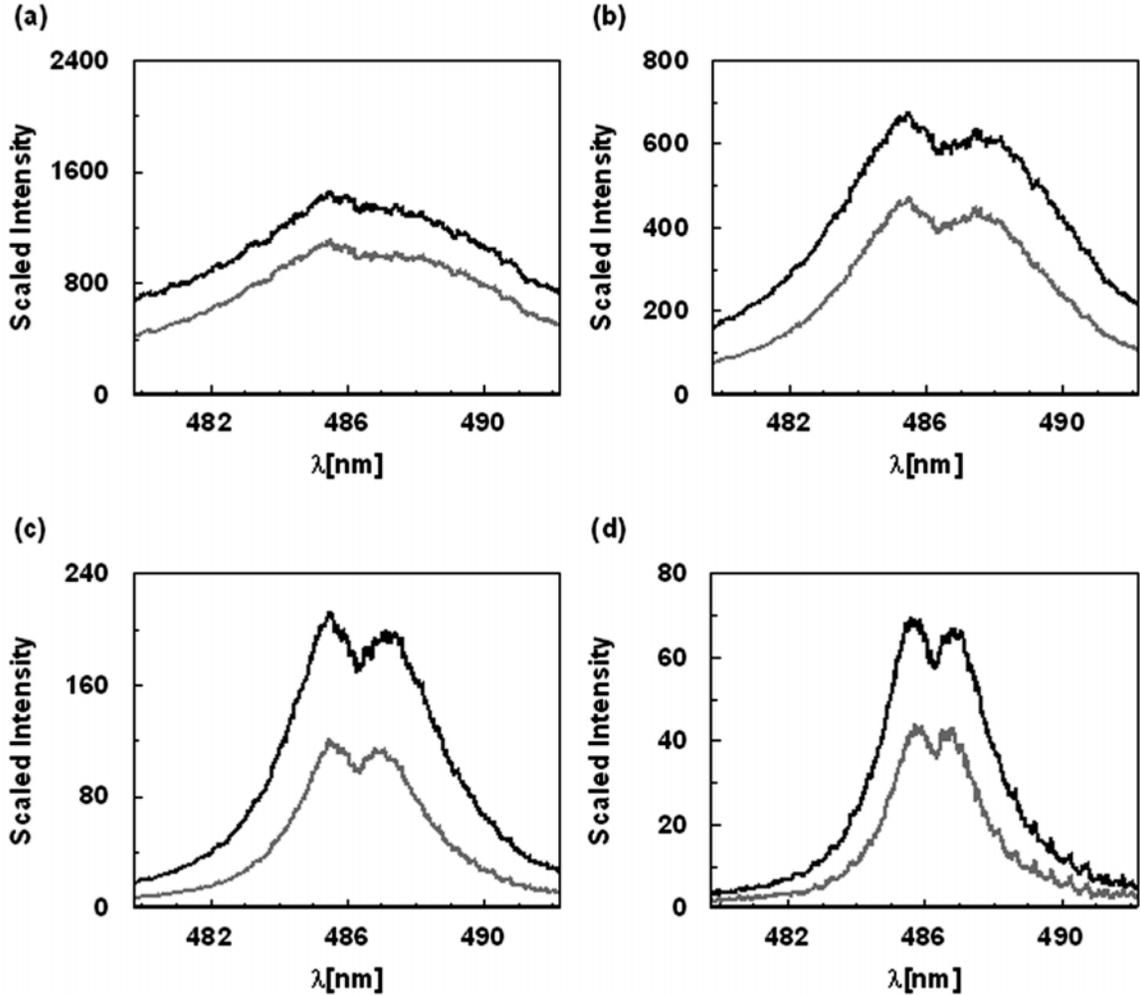

Fig. 7: Hydrogen-beta emissions in expanding methane flow at 2.7×10^5 Pa. Time delays (a) $t_{delay} = 0.3$ µs (top), 0.4 µs, (b) $t_{delay} = 0.6$ µs (top), 0.8 µs, (c) $t_{delay} = 1.2$ µs (top), 1.5 µs, (d) $t_{delay} = 1.8$ µs (top), 2.1 µs. Note weak (particularly near 490-nm) presence of the $C_2 \, d^3\Pi_g \rightarrow \Pi_u$ swan system $\Delta v = 0$ sequence for time delays > 1.5 µs in Fig. (d)
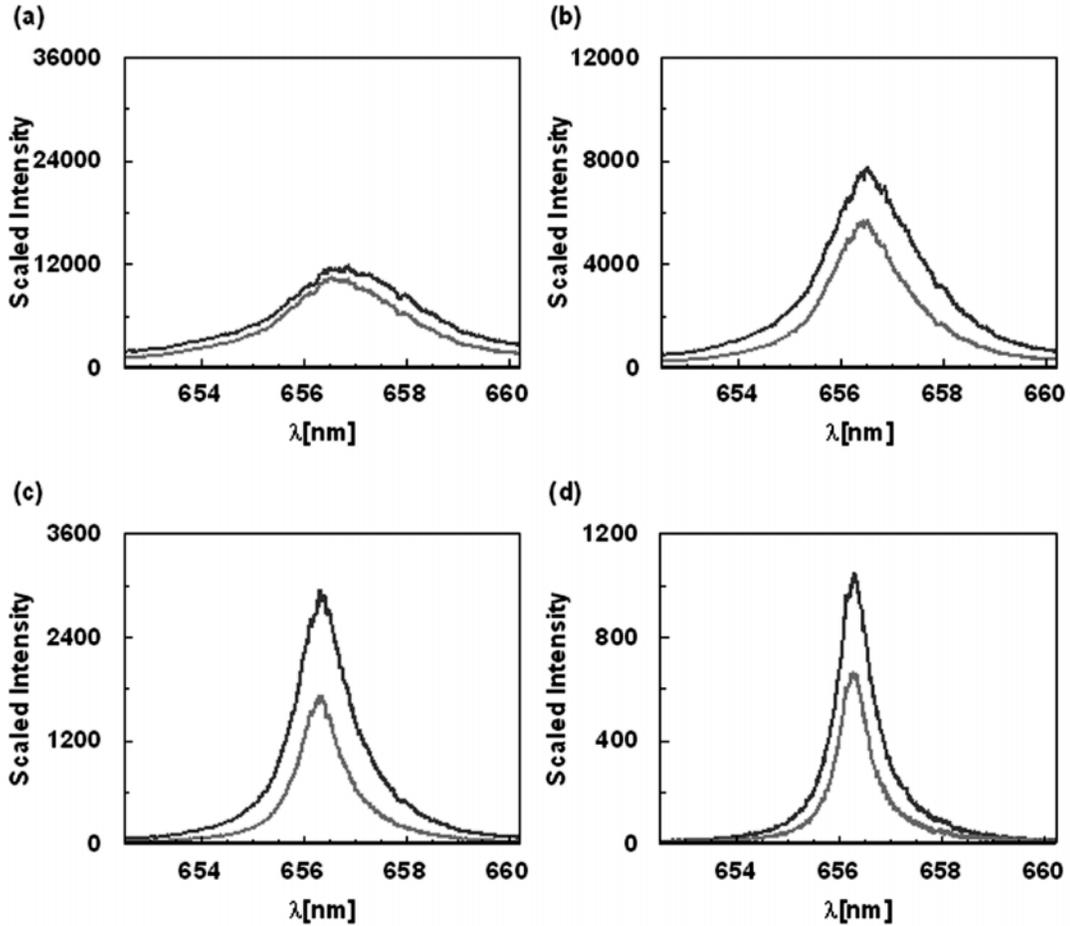
Fig. 8: Hydrogen-alpha emissions in expanding methane flow at 2.7×10^5 Pa. Time delays (a) $t_{delay} = 0.3$ µs (top), 0.4 µs, (b) $t_{delay} = 0.6$ µs (top), 0.8 µs, (c) $t_{delay} = 1.2$ µs (top), 1.5 µs, (d) $t_{delay} = 1.8$ µs (top), 2.1 µs

0.25 ± 0.03 nm and 0.29 ± 0.03 nm, for electron number density of $N_e = 10 \times 10^{17}$ cm^{-3} [31].

Applications of Stark-broadening include H-alpha, H-beta, and H-gamma (H_α: 6562.8 Å, H_β: 4861.4 Å, H_γ: 4340.5 Å) diagnostic of LIOB in methane [32–34]. Figures 6–8 show spectra for H_α, H_β and H_γ recorded in expanding methane flow at a pressure of 2.7×10^5 Pa. For these experiments, we used a 100-ns gate width to evaluate electron density following LIOB. A 100-ns gate (or intensifier) limits somewhat study of early plasma decay due to the previously debated temperature variation [27, 28] early in the plasma decay. Nevertheless, the Boltzmann plot method was applied to extract temperature. Figure 9, shows the inferred temperature versus time delay from LIOB. Clearly, there are significant uncertainties due to use of incomplete atomic line profiles. And of course uncertainties result from the temperature gradient early after LIOB when a gate-width of 100-ns is utilized, indicated by the horizontal error bars.
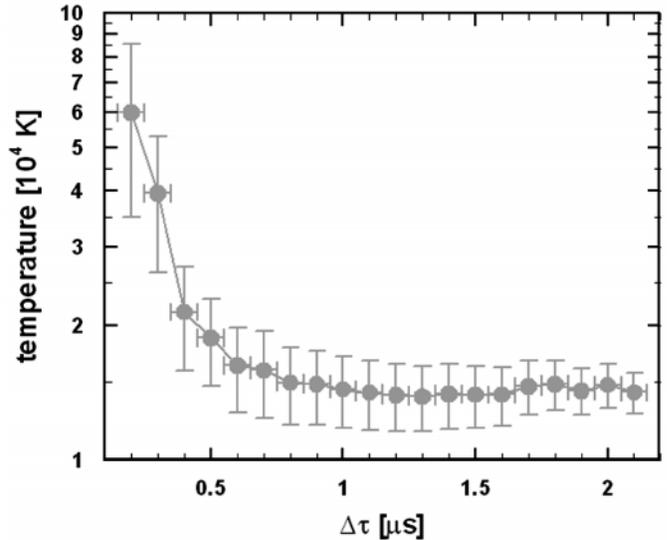
Fig. 9: Temperature versus time delay from LIOB, inferred from Boltzmann plots. The vertical error bars reflect the uncertainty in determining Boltzmann plots from incomplete line profiles (see Figs 6–8)

H-alpha, H-beta and H-gamma measurements. Once again, early in the plasma decay, the Boltzmann-plot inferred temperatures [34] in the range of 30,000 to 10,000 K for delays of 0.4 to 2.1 µs from LIOB, shows relatively large errors due to recording of incomplete line profiles. The inferred temperature and uncertainties for earlier delays of 0.2 and 0.3 µs show relatively large variations due to the choice of 100-ns gate-width as well. In addition, self absorption [34] is noted for recorded line profiles early in the plasma decay. Tables 6 and 7 show selected results for the three Balmer lines H_α, H_β and H_γ.

Table 6
Measured (FWHM) for H_α, H_β and H_γ lines in CH_4 flow at 2.7×10^5 Pa

| Time Delay [µs]	H_α Width [nm]	H_β Width [nm]	H_γ Width [nm]
0.4	2.8 ± 0.3	10.0 ± 0.9	11.0 ± 2.0
0.6	2.1 ± 0.3	8.1 ± 0.7	8.7 ± 1.5
1.2	1.2 ± 0.1	5.0 ± 0.3	5.8 ± 1.0
1.5	1.0 ± 0.1	4.1 ± 0.3	5.2 ± 1.0
1.8	0.79 ± 0.1	3.6 ± 0.2	5.0 ± 1.0

Table 7
Deduced N_e from FWHM (Table 6) for H_α, H_β and H_γ lines

Time Delay [µs]	H_α N_e [10^{17} cm^{-3}]	H_β N_e [10^{17} cm^{-3}]	H_γ N_e [10^{17} cm^{-3}]
0.4	5.0 ± 0.4	2.9 ± 0.8	2.4 ± 0.7
0.6	3.0 ± 0.4	2.2 ± 0.6	1.9 ± 0.5
1.2	1.3 ± 0.2	1.1 ± 0.5	1.1 ± 0.3
1.5	1.0 ± 0.2	0.79 ± 0.3	0.92 ± 0.3
1.8	0.72 ± 0.1	0.68 ± 0.2	0.90 ± 0.3

The primary contribution in the error bars originates from experimental widths. Other contributions to the error bars comprise uncertainty in the temperature and the uncertainty in the reduced mass of the pairs "perturber-radiator" the LIOB discharge occurs in methane (CH_4), so the perturbers could be not only hydrogen ions (protons), but also carbon ions. The reduced mass is $\mu = 0.5$ for the pairs H–H or $\mu = 0.923$ for the pairs H–C$^+$ and H–C^{++}.

Detailed curve fitting [8, 43, 44] of the H-beta line using line-profiles based on the so-called Vidal-Cooper-Smith (VCS) unified theory shows deficiencies in predicting the H_β center-dip. Ion-dynamical correction

in the computational model [43] shows notable improvements in the residuals. Figure 10 shows a typical result when using Zîkić et al. [43] computational model curve fitting.
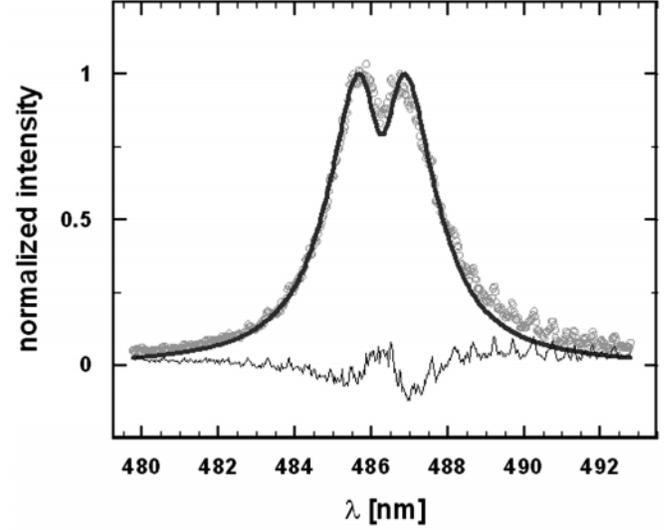
Fig. 10: Results of H-beta fitting using symmetric profiles from Zîkić et al. [43]. Time delay from LIOB $\Delta\tau = 2.0$ µs, $\Delta\lambda_{FWHM} = 3.2$ nm, $N_e = 0.56 \times 10^{17}$ cm^{-3}, $T_e = 1.2 \times 10^4$ K, reduced mass $\mu = 0.93$

The inferred electron densities also agree when using full-width-half maximum (FWHM) or full-width-half-area (FWHA) for the H_α, H_β and H_γ lines [34]. Recently predicted asymmetrical line profiles [35] for H-beta line profiles show agreement with measured peak-separation of the double-peak H_β profiles [27]. Applications of hydrogen Balmer series measurements including spatial and temporal characteristics of LIOB will be of continued interest in LIBS and/or LIPS [18–21, 45–49].

4. CONCLUSIONS

Measurements of the electron density of up to 10^{19} cm^{-3} were possible using the H_α spectral line. Use of the H_β spectral line for determination of the electron density is limited to approximately less than 6×10^{17} cm^{-3} due to the typically by a factor of 4 broader hydrogen-beta line than the hydrogen-alpha line, for otherwise identical plasma conditions, and due to the spectral proximity of other Balmer series lines such as H_δ. Uncertainties in determining the electron temperature early in the plasma decay, by use of Boltzmann plots, are caused by extreme broadening and partial overlap of the H_α, H_β, and H_γ, spectral lines. In fact, values for the temperature were determined only for time delays longer

than 0.25 µs following optical breakdown. This in turn results in uncertainties of the electron densities.

Use of Oks' SBT/theory allows one to eliminate the discrepancies that would result when using Griem's SBT/theory to determine the electron density N_e from H_α and H_β width measurements. Moreover, the values N_e obtained from the H_α shift using Oks' theory also agrees with the corresponding values of N_e inferred from the widths. We note that the employment of SBT/simulations by GC/GGC would still lead to noticeable discrepancies between the values of N_e deduced from H_α and H_β width measurements.

Although the presented experimental results for H_α, H_β and H_γ lines, with the use of Oks' SBT/theory to determine electron density, nicely agree within the experimental errors, further experimental studies are of interest — for example, designing a modified setup that ideally would measure simultaneously spectrally and temporally well-resolved Balmer-series hydrogen lines subsequent to laser-induced optical breakdown. In the studies presented here emphasis was on the early plasma-decay, with line-widths significantly larger than instrument or Doppler widths. So, to further address discrepancies that might exist at the lowest experimental density range, or for time delays longer than 2 µs from optical breakdown, highly spectrally and spatially resolved data are desirable. Yet in turn, the onset of fluid physics phenomena, as can be seen from the shadowgraphs, will pose experimental challenges due to development of expected electron density gradients as the plasma expands.

REFERENCES

[1] H.R. Griem, "Plasma Spectroscopy", (McGraw-Hill, New York) 1964.

[2] H.R. Griem, "Spectral Line Broadening by Plasmas", (Academic Press, New York) 1974.

[3] I.I. Sobelman, L.A. Vainshtein, and E.A. Yukov, "Excitation of Atoms and Broadening of Spectral Lines", (Springer, Berlin) 1995.

[4] H.R. Griem, "Principles of Plasmas Spectroscopy", (Cambridge University Press, New York) 1997.

[5] T. Fujimoto, "Plasma Spectroscopy", (Clarendon Press, Oxford) 2004.

[6] E. Oks, "Stark Broadening of Hydrogen and Hydrogenlike Spectral Lines on Plasmas". The Physical Insight (Alpha Science International, Oxford) 2006.

[7] M.A. Gigosos and V. Cardeñoso, "J. Phys. B", **29**, 4795, (1996).

[8] M.A. Gigosos, M.Á. González, and V. Cardeñoso, "Spectrochim. Acta B: Atomic Spectrosc", **58**, 1489, (2003).

[9] E. Oks, in Proc. 18th Intern. Conf. Spectral Line Shapes, AIP Conf. Proceedings 874 (American Institute of Physics, New York) 2006, pp. 19.

[10] M.M. Litvak and D.F. Edwards, "IEEE J. Quantum Electron, QE", **2**, 486, (1966).

[11] W.L. Wiese, D.E. Kelleher, and D.R. Paquette, "Phys. Rev. A", **6**, 1132, (1972).

[12] V. Helbig and K.P. Nick, "J. Phys. B", **14**, 3573, (1981).

[13] W.L. Wiese and J.A. Augis, "J. Appl. Phys.", **48**, 4528, (1977).

[14] J.H. Eickmans, W.F. Hsieh, and R.K. Chang, "Appl. Opt.", **26**, 3721, (1987).

[15] J. Ashkenazy, R. Kipper, and M. Caner, "Phys. Rev. A", **43**, 5568, (1991).

[16] P. Blau, I. Smilanski, and S. Rosenwaks, "J. Appl. Phys.", **72**, 849, (1992).

[17] J.B. Simeonsson and A.W. Miziolek, "Appl. Opt.", **32**, 939, (1993).

[18] L.J. Radziemski, D.A. Cremers, eds. "Laser-Induced Plasmas and Applications", (Marcel Dekker, New York) 1989.

[19] A.W. Miziolek, V. Palleschi, I. Schechter, eds. "Laser Induced Breakdown Spectroscopy", (Cambridge University Press, New York) 2006.

[20] D.E. Cremers, Leon J. Radziemski, "Handbook of Laser-Induced Breakdown Spectroscopy", (John Wiley, New York) 2006.

[21] J.P. Singh, S.N. Thakur, eds., "Laser Induced Breakdown Spectroscopy", (Elsevier Science, New York) 2007.

[22] J. Pender, B. Pearman, J. Scaffidi, S.R. Goode, and S.M. Angel, "Laser-induced Breakdown Spectroscopy using Sequential Laser Pulses", Chapter 15 in A.W. Miziolek, V. Palleschi, I. Schechter, eds., "Laser Induced Breakdown Spectroscopy" (Cambridge University Press, New York) 2006.

[23] D.K. Killinger, S.D. Allen, R.D. Waterbury, C. Stefano, and Edwin L. Dottery, "Opt. Expr.", **15**, 12905, (2007).

[24] C. López-Moreno, S. Palanco, J.J. Laserna, F. DeLucia Jr, A.W. Miziolek, J. Rose, R.A. Walters and A.I. Whitehouse, "J. Anal. At. Spectrom", **21**, 5560, (2006).

[25] M.Z. Martin, M-D Cheng, and R.C. Martin, "Aerosol Sciences and Technology", **31**, (1999), 409.

[26] C.G. Parigger, "Laser-induced Breakdown in Gases: Experiments and Simulation", Chapter 4 in A.W. Miziolek, V. Palleschi, I. Schechter, eds., "Laser Induced Breakdown Spectroscopy", (Cambridge University Press, New York) 2006.

[27] C.G. Parigger, D.H. Plemmons, and E. Oks, "Appl. Opt.", **42**, 5992, (2003).

[28] C. Parigger, J.W.L. Lewis, and D.H. Plemmons, "J. Quant. Spectrosc. Radiat. Transfer", **53**, 249, (1995).

[29] C. Parigger, D.H. Plemmons, and J.W.L. Lewis, "Appl. Opt.", **34**, 3325, (1995).

[30] C.G. Parigger, in Proc. 18th Intern. Conf. Spectral Line Shapes, AIP Conf. Proceedings 874 (American Institute of Physics, New York) pp. 101, (2006).

[31] C.G. Parigger, J.O. Hornkohl, and L. Nemes, "Appl. Opt.", **46**, 4026, (2007).

[32] C.G. Parigger, M. Dackman, and J.O. Hornkohl, "Appl. Opt.", **47**, G1 (2008).

[33] C.G. Parigger and E. Oks, "Int. J. Spectroscopy", 2010, 936385, (2010).

[34] C.G. Parigger and E. Oks, submitted to "Appl. Opt.", (2009).

[35] S. Djurović, M. Ćirišan, A.V. Demura, G.V. Demchenko, D. Nikolić, M.A. Gigosos, and M.Á. González, "Phys. Rev. E", **79**, 046402, (2009).

[36] G.S. Settles, "Schlieren and Shadowgraph Techniques: Visualizing Phenomena in Transparent Media", (Springer Verlag, New York) 2001.

[37] T.X. Phuoc, "Opt. Commun.", **175**, 419, (2000).

[38] A.E. Siegman, "Lasers," (University Science, Mill Valley, CA) 1986.

[39] R.N. Compton, J.C. Miller, "Multiphoton Ionization Photoelectron Spectroscopy MPI-PES", Chapter 6 in D.K. Evans ed., Laser Applications in Physical Chemistry (Marcel Dekker, New York) 1989.

[40] I.G. Dors, C.G. Parigger, "Appl.Opt.", **42**, 5978, (2003).

[41] C.G. Parigger, G. Guan, J.O. Hornkohl, "Appl.Opt.", **42**, 5986, (2003).

[42] O. Renner, D. Salzmann, P. Sondhauss, A. Djaoui, E. Krouský and E. Förster, "J. Phys. B", **31**, 1379, (1998).

[43] R. Z ki , M.A.Gigosos, M.Ivković, M.Á.González, N.Konjević, "Spectrochim. Acta B: Atomic Spectrosc", **57**, 987, (2002).

[44] M.Á. González and M.A. Gigosos, "Plasma Sources Sci. Technol.", **18**, 034001, (2009).

[45] J.A. Aguilera and C. Aragón, "Spectrochim. Acta B: Atomic Spectrosc", **59**, 1861, (2004).

[46] A.J. Ball, V. Hohreiter, and D.W. Hahn, "Appl. Spectrosc", **59**, 348, (2005).

[47] A. De Giacomo, M. Dell'Aglio, R. Gaudiuso, G. Cristoforetti, S. Legnaioli, V. Palleschi and E. Tognoni, "Spectrochim. Acta B: Atomic Spectrosc", **63**, 980, (2008).

[48] H-Y Moon, K.K. Herrera, N. Omenetto, B.W. Smith, and J.D. Winefordner, "Spectrochim. Acta B: Atomic Spectrosc", **64**, 702, (2009).

[49] U. Panne and K. Niemax, "Spectrochim. Acta B: Atomic Spectrosc", **64**, 929, (2009), and see recent articles in this 2009 feature issue on LIBS.